JOURNAL OF SOLID STATE CHEMISTRY 119, 224–236 (1995)

Synthesis Structure and Superconductivity in All-Perovskite-Layered Titanium Cuprates[1]

M. R. Palacín, A. Fuertes, N. Casañ-Pastor, and P. Gómez-Romero[2]

Institut de Ciència de Materials de Barcelona (CSIC), Campus UAB, E-08193 Bellaterra, Barcelona, Spain

Received September 7, 1994; in revised form April 27, 1995; accepted May 2, 1995

A study on the reaction pathways, the synthesis, and the range of stability of complex perovskites in the system *Ln*–(Sr/Ba)–Cu–Ti is reported. Several possibilities for the Cu : Ti stoichiometry were explored with the aim of isolating potentially superconducting layered phases. A bulk superconducting phase of the formula $YSr_2Cu_{2.7}Ti_{0.3}O_{8-\delta}$ with a T_c of 26 K was isolated and a whole family of layered oxides of the formula $Ln_2Ba_2Cu_2Ti_2O_{11-\delta}$ was characterized. We have determined the limits of this family which extends from *Ln* = La to Tb. The studies reported include X-ray and electron diffraction, and TGA and magnetic susceptibility measurements. Structural and magnetic correlations for these oxides are analyzed. © 1995 Academic Press, Inc.

INTRODUCTION

Based on the experience gained with the large number of cuprate superconductors reported to date, it is now widely accepted that a necessary condition for high-*Tc* superconductivity is the existence of layers of corner-sharing Cu–O polyhedra within the structure of these oxides. For the induction of this required bidimensionality, the approach most frequently used seeks the formation of intergrowths between copper-based perovskite layers and structurally compatible blocks where other metals and oxygen form a structure similar to that of NaCl.

An alternative approach which we have explored for the induction of bidimensionality is the formation of mixed perovskites of copper and other metals with the aim of segregating layers of copper polyhedra within an "all-perovskite" framework. This requires developing ways to control the structure and order in these oxides.

After the early discovery of $YBa_2Cu_3O_{7-\delta}$ (1), which is a most unique example of this kind of layered perovskite segregation, many reports of small level substitutions ("doping") of copper appeared in the literature. On the other hand, work on new all-perovskite phases has been developed only very recently. First, a series of studies on new phases directly derived from $YBa_2Cu_3O_{7-\delta}$ have been appearing where the Cu1 ions, forming CuO chains, are totally replaced by other metals such as Nb and Ta (2–7), Al (8), Fe (9), Ga (10–13) or Co (12–17); other related perovskites containing iron but no copper are also known (18–20). Several reports dealing with the study of simpler perovskite structures (*LnA*Cu*M*O5) containing either Fe (21–23) or Co (24, 25) have also been published. From a solid state chemistry point of view, however, the most striking novelties have been, the report of a three-dimensional perovskite with alternating layers of copper and tin ions (26), and a more recent report of a novel layered perovskite superstructure also based on copper and tin (27), neither of which have led yet to superconducting systems.

Our recent work in this field has centered on the study of mixed perovskites of copper and early transition elements, and specifically on the effects of different synthetic strategies on the formation, structure, and properties of these oxides (28–31). This approach has led us to explore the formation of three-dimensional as well as layered phases with perovskite-related structures in the system *Ln*–(Sr/Ba)–Cu–Ti (28). We have recently reported the successful induction of bidimensionality in mixed copper–titanium perovskites with the synthesis of a series of oxides of formula $Ln_2Ba_2Cu_2Ti_2O_{11}$ (*Ln* = La,Nd,Eu (32, 33) and *Ln* = Tb (34)). An independent report on the related compound with *Ln* = Gd has also recently appeared (35). The present work reports our main results in the search for new layered titanium cuprates of the perovskite family concerning the study of synthetic reactions, the isolation of new phases, their characterization and the study of structural correlations.

EXPERIMENTAL

All samples were prepared by solid state reaction of stoichiometric amounts of TiO_2, CuO, $BaCO_3$, or $SrCO_3$ and Ln_2O_3 (*Ln* = La, Nd, Eu, Tb, Dy, Y) or $Tb_2(CO_3)_3$, all of them purchased from Aldrich or Baker and of purity ≥99.9%. To ensure the purity of the reagents (they can

[1] This work constitutes part of M. R. Palacín's Ph.D. Thesis.

[2] To whom correspondence should be addressed.

0022-4596/95 $12.00

absorb H_2O and CO_2 from air (36)), Ln_2O_3 was treated at 1000°C for 15 hr and $BaCO_3$ and $SrCO_3$ were treated at 200°C for 2 days. The syntheses were carried out in two steps of 24 hr each with an intermediate regrinding, the first step consisted of 2 hr at 900°C to allow the carbonates to decompose plus 24 hr at the temperature of reaction. The second step consisted of a single heating run at the temperature of reaction for 24 hr. In some cases, this step was repeated to make sure that the reaction was complete. Reactions were carried out in air, the temperature of synthesis was usually 1100°C but in some cases other temperatures between 900°C and 1200°C were also tried in order to study the effect of the temperature on the reaction products. Heating and cooling rates were 100°C/hr.

Some samples were further annealed under flowing oxygen at 500°C for 48 hr and with a cooling rate of 30°C/hr. When sintering was necessary, it was performed at the synthesis temperature for 15 hr just before the annealing process.

The progress of the reaction was followed by X-ray powder diffractometry, and this technique was also used to characterize structurally these new phases. X-ray powder diffraction patterns were obtained using Cu$K\alpha$ radiation, with both a Siemens D-500 diffractometer (λ = 1.5418 Å) and a Rigaku D/MAX-RC rotating-anode diffractometer (RU 200-B) generator featuring monochromatized (Ge 1,1,1) radiation (λ = 1.5405 Å).

Electron Diffraction patterns and low resolution images were obtained using a JEOL JEM-1210 microscope operating at 120 kV, equipped with a side-entry 60°/30° double-tilt GATHAN 646 analytical specimen holder and a Link QX2000 EDX element analysis system. The specimens for electron microscopy were prepared by grinding the powder sample, dispersing it in *n*-butanol, and depositing a droplet of this suspension on a carbon coated holey film supported on an aluminum grid. For EDX analysis the specimen was held at the optimum degree of tilt toward the X-ray detector, $x = +20$, $y = -20$. Typically, 10 small crystals were analyzed at 100,000× with a counting time of 100 sec and the intensities were obtained from the spectra by making appropriate background subtractions, measuring the background on each side of the peaks. The proportionality constants were determined by analyzing well-characterized standard samples. In the case of problem samples containing both barium and titanium, where extensive overlap takes place, a subtraction of the barium contribution was necessary in order to evaluate the amount of titanium present.

The determination of the oxygen content of the samples was carried out by thermogravimetric analyses under Ar–H_2 (5% H_2 v/v) at 650°C, performed with a PE TGA7 balance (maximum sensitivity 0.1 μg) and normally with ca. 40 mg of sample.

Magnetic susceptibility data were collected on a Quantum Design SQUID magnetometer, with an applied field of 10,000 G. In the case of superconducting samples the magnetic field was 5 G and was applied after the sample was cooled in the absence of field (zero field cooling).

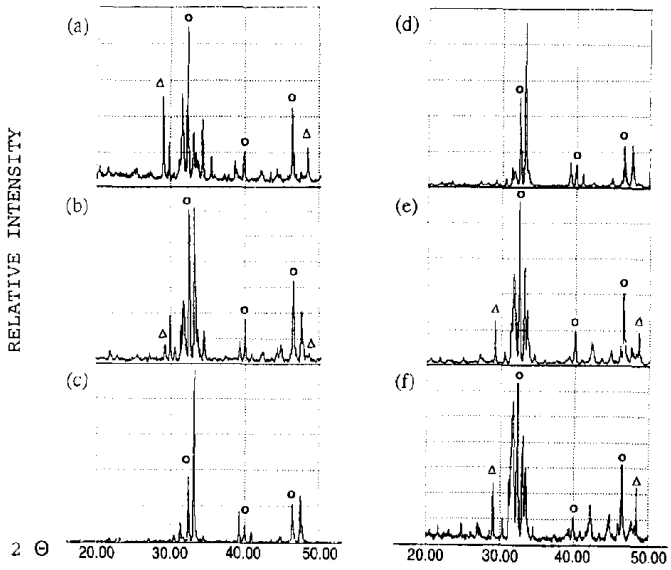

FIG. 1. X-ray diffraction patterns for samples of nominal composition $YSr_2Cu_2TiO_{8-\delta}$ synthesized at (a) 980, (b) 1000, (c) 1025, (d) 1050, (e) 1075, and (f) 1100°C. The symbols △ and ○ indicate the peaks corresponding to Y_2O_3 and $SrTiO_3$, respectively.

RESULTS AND DISCUSSION

Sr-1221 Samples: Nominal Composition $LnSr_2Cu_2TiO_{8-\delta}$ (Ln = La, Nd, Eu, Y)

For this series of nominal compositions we tested several reaction conditions to try to obtain a pure phase with cationic stoichiometry 1221 that would have a 123-type structure (temperatures of synthesis ranging from 980 to 1100°C). In spite of this we obtained in all cases a mixture of phases as a result of the reaction.

The results were different for *Ln* = La, Nd, or Eu than for *Ln* = Y. For the first three ions mixtures of different ternary oxides were obtained for all the reaction temperatures tried, whereas for *Ln* = Y the results depended very much on the temperature, as shown in Fig. 1. For temperatures lower than 1025°C, the reaction product contained mainly $SrTiO_3$ and a perovskite-type phase and also Y_2O_3 and $SrCuO_2$. For samples prepared at 1025°C the powder diffraction pattern showed the perovskite-type phase as the major product, although the sample contained a considerable amount of $SrTiO_3$ and also a small amount of Y_2O_3 and $SrCuO_2$. For temperatures higher than 1025°C the results obtained were similar to those found below 1025°C. Thus, the formation of the

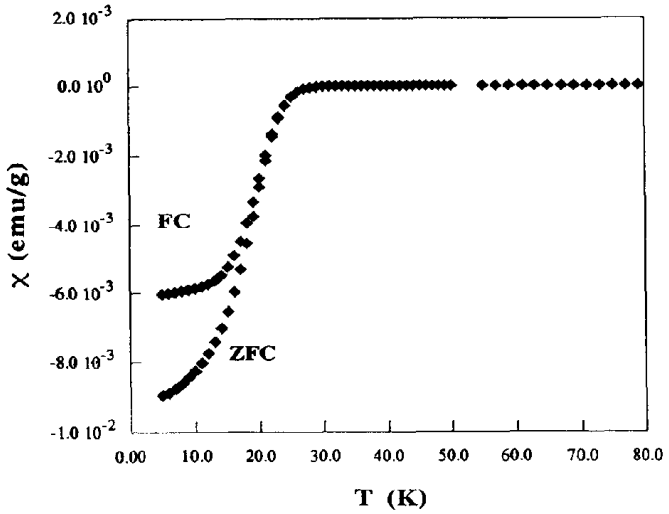

FIG. 2. Plot of zero field cooling and field cooling magnetic susceptibility (H = 10 G) as a function of temperature for a sample with the optimized composition $YSr_2Cu_{2.7}Ti_{0.3}O_{8-\delta}$ (δ = 0.94), synthesized at 1035°C and annealed under oxygen at 500°C. It shows a superconducting transition with an onset at 26 K and 80% Meissner fraction.

perovskite-type phase depends very much on the temperature of the reaction, being optimal at 1035°C.

Susceptibility measurements made on an oxygen-annealed sample showed a superconducting transition with a $T_{c\,(onset)}$ = 26 K (Fig. 2). The observed Meissner effect corresponds in this case to ca. 80% of the ideal $1/4\pi$ diamagnetism, indicating bulk superconducting behavior. The chemical nature of this sample was investigated by EDX analyses and its crystal symmetry by electron diffraction and low-resolution imaging.

Electron diffraction studies of the sample synthesized at 1035°C revealed that the major perovskite-type phase presents an $a_p \times a_p \times 3a_p$ superstructure (see Fig. 3). The same figure shows a low-resolution image corresponding to the [100] zone axis. The reconstruction of the reciprocal lattice indicates that the symmetry is tetragonal and without systematic absences, thus corresponding to the extinction symbol P---. EDX data on this sample were collected and a quantitative analysis was performed with the aid of ternary oxides as standards ($Y_2Cu_2O_5$, $SrTiO_3$, and Sr_2CuO_3). The analysis of the crystals with the $a_p \times a_p \times 3a_p$ superstructure gave a composition of $Y_{0.9}Sr_{2.2}Cu_{2.7}Ti_{0.4}O_X$ with an uncertainty of about 10% in the stoichiometric coefficients.

The fact that the sample is a bulk superconductor indicates that the yttrium strontium copper titanium oxide with the $a_p \times a_p \times 3a_p$ superstructure is responsible for this behavior. Den and Kobayashi (37a), and in a more recent paper, Wuu *et al.* (37b) have reported a superconducting phase of formula $YSr_2Cu_{2.7}Ti_{0.3}O_{7+\delta}$ with T_c values (at atmospheric pressure) of 26 K (37a) and up to 35 K (37b), but with values heavily dependent on the oxidation level. We have found a coincident superconducting behavior which, together with the similar range of stability found for this phase, strongly suggests that both phases are the same.

Ba-1221 Samples: Nominal Composition $LnBa_2Cu_2TiO_{8-\delta}$ (Ln = La, Nd, Eu, Y)

In the case of A = Ba and Ln = Y the product of the reaction was a mixture of ternary and quaternary oxides no matter which temperature of synthesis was used. On the other hand, in the case of A = Ba and Ln = La, Nd, Eu, a perovskite-type phase was clearly predominant and there was also a small amount of impurities with main reflections at $2\theta \sim 30$. Figure 4 shows the X-ray diffraction patterns from samples with nominal composition 1221 synthesized at 1100°C. In order to eliminate these impurities we also tried the syntheses with different Ln : A ratios

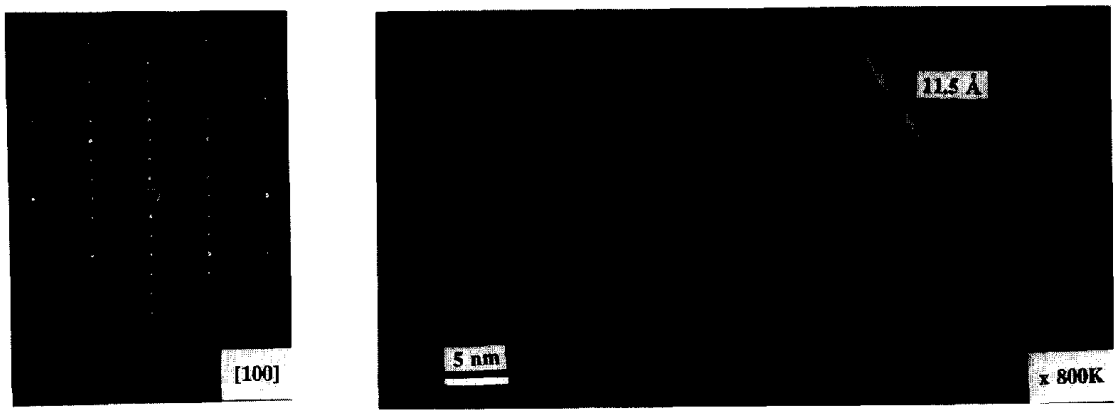

FIG. 3. Electron diffraction pattern and low resolution image corresponding to the [100] zone axis for a crystal of the superconducting $YSr_2Cu_{2.7}Ti_{0.3}O_{8-\delta}$ sample.

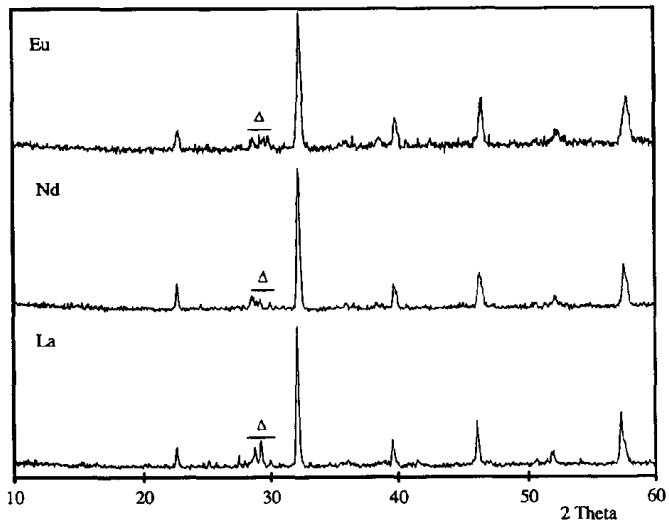

FIG. 4. X-ray diffraction patterns for samples of nominal composition LnBa$_2$Cu$_2$TiO$_{8-\delta}$ (Ln = La, Nd, and Eu) synthesized at 1100°C. The symbol Δ indicates the peaks which correspond to impurities of BaCuO$_2$ and Ln_2BaCuO$_5$.

(Ln_{1+x}Ba$_{2-x}$Cu$_2$TiO$_{8-\delta}$, x = 1, 0.8, 0.7, 0.6, 0.5, 0.4, 0.2, 0.1, and 0) but there were always some small peaks at $2\theta \sim 30$. The nature of these impurity phases depends on the nominal composition; for Ba-rich samples they consist of barium copper oxides and for Ln-rich samples of lanthanide copper oxides.

We performed electron diffraction on these samples in order to find out whether the main perovskite phase was indeed a 123-type structure with a c axis three times that of a simple perovskite. The results clearly showed that the major phase had a structure derived from that of the perovskite with a fourfold superstructure, which we assigned to the phase Ln_2Ba$_2$Cu$_2$Ti$_2$O$_{11-\delta}$ (referred to as the 2222 phase). This result is consistent with the absence of titanium in the impurities. The reaction taking place in the sample with 1221 stoichiometry would then be

$$0.5Ln_2O_3 + 2BaCO_3 + 2CuO + TiO_2 \xrightarrow{-2CO_2} 0.5Ln_2Ba_2Cu_2Ti_2O_{11-\delta} + BaCuO_2.$$

With this particular example we would like to remark upon the great importance of electron diffraction in the characterization of perovskite-type oxides and the risk of reaching structural conclusions based on X-ray powder diffractometry alone. In this sense, a report on the physical properties of samples with stoichiometry LnBa$_2$Cu$_{3-x}$Ti$_x$O$_{7+\delta}$ (Ln = La–Gd, Y, $0 \le x \le 1$) has been published recently (38). The authors claim to have obtained a 123-type structure relying only on powder diffraction patterns. According to their interpretation of those data their sample would contain a 123-type phase with a small amount of impurities at $2\theta \sim 30$. The diffraction patterns of their products and the nature of the impurities they obtain are indeed the same as ours, so we believe their samples might also contain the phase with $4a_p$ superstructure in addition to or, more likely, instead of the 123-type structure, thus compromising the interpretation of the abundant data reported on transport and magnetic properties.

In our case, an exhaustive analytical study has been necessary for the correct interpretation of physical measurements conducted on the sample with nominal composition Eu$_{1.4}$Ba$_{1.6}$Cu$_2$TiO$_{8-\delta}$. This sample presented a superconducting transition with an onset at about 50 K. The transition was apparent both from magnetic and transport measurements (28). However, the Meissner fraction was only 1% of the ideal value $1/4\pi$. In order to optimize the superconducting properties an unambiguous assignment of the phase responsible was necessary. This took the careful analyses of electron diffraction and EDX data; the former allowed the detection of small amounts of an $a_p \times a_p \times 3a_p$ phase which by EDX analyses was found to contain Eu, Ba, and Cu in an approximate 1 : 1 : 2 ratio but no Ti. This combination of composition and properties agrees closely with those of formerly reported superconducting phases of formula La$_{1.4}$Ba$_{1.6}$Cu$_3$O$_{7-\delta}$ (39) and Nd$_{1.4}$Ba$_{1.6}$Cu$_3$O$_{7-\delta}$ (40), which most likely constituted the superconducting impurity detected in our sample.

Based on all the above results, we can conclude that a straightforward one-to-one substitution of Ti for Cu in the structure of LnBa$_2$Cu$_3$O$_{7-\delta}$ to yield LnBa$_2$Cu$_2$Ti$_2$O$_x$ is unlikely. Some attempts have been made to obtain such a substitution (38, 41, 42) and indeed some similar structures are known with Nb or Ta replacing Cu (2–7). Nevertheless, in the case of titanium this phase would be especially difficult to prepare under ordinary synthetic conditions (in air), since a hypothetical LnBa$_2$Cu$_2$TiO$_{8-\delta}$ would contain copper in a formal oxidation state of 2.5 (assuming Ti(IV)) and this seems difficult to achieve unless high-pressure synthetic methods were used. In fact, attempts to synthesize the isovalent oxide LaBa$_2$Cu$_2$SnO$_8$ have also failed (27), leading to mixtures where the major product of the reaction is the Sn-2222 phase, similar to what we have found in the Cu–Ti systems. On the other hand, we must note how the oxide reported by Den and Kobayashi and later by Wuu et al., which we have also found in our studies, contains copper in an average formal oxidation state of 2.34, similar to what is found for YBa$_2$Cu$_3$O$_7$, with both systems being prepared under a P_{O_2} of 1 atm.

Synthesis of $Ln_2Ba_2Cu_2Ti_2O_{11-\delta}$ (Ln = La, Nd, Eu, Tb, Dy, Y)

In contrast to the results with 1221 compositions, these compounds could be obtained as essentially pure phases

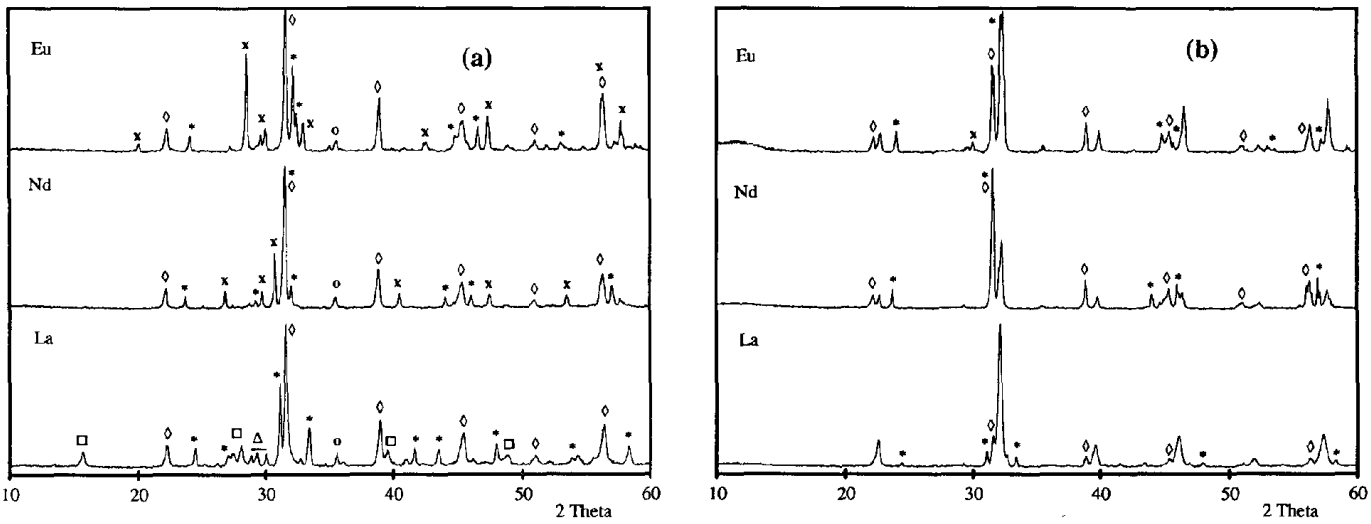

FIG. 5. X-ray diffraction patterns of stoichiometric mixtures of Ln_2O_3, $BaCO_3$, CuO, and TiO_2 treated at (a) 900 and (b) 1000°C. The symbols stand as follows: *, Ln_2CuO_4; △, $BaCuO_2$; × Ln_2O_3; ○, CuO, □, $Ln(OH)_3$; and ◇, $BaTiO_3$. Peaks without symbols correspond to $Ln_2Ba_2Cu_2Ti_2O_{11-\delta}$.

with the only limitation being their relative stability versus that of the corresponding ternary oxides (see below). These oxides were also detected on reaction mixtures with nominal compositions $Ln_1Ba_2Cu_2Ti_1$, as mentioned above.

We present here our studies on the influence of the synthetic conditions, namely temperature and time, on the products obtained upon reaction of the corresponding oxides and carbonates.

For Ln = La, Nd, and Eu, we performed the reaction at 900, 1000, and 1100°C in two steps of 24 hr with an intermediate regrinding in each case. Figures 5a and 5b show the X-ray powder patterns of the products obtained at 900 and 1000°C to illustrate the effect of temperature on the progress of the reaction. We can see that at 900°C the product of the reaction is a mixture of phases, containing mainly starting products and $BaTiO_3$, Ln_2CuO_4, and CuO; under these conditions the initial reaction taking place would then be

$$Ln_2O_3 + 2BaCO_3 + 2CuO + 2TiO_2 \xrightarrow{-2CO_2} 2BaTiO_3 + Ln_2CuO_4 + CuO.$$

When the reaction takes place at 1000°C, and following the procedure described under Experimental, a mixture containing the same intermediate oxides and a considerable amount of the 2222 phase is obtained. In the case of lanthanum the reaction seems to proceed faster and the main phase is already $La_2Ba_2Cu_2Ti_2O_{11-\delta}$. If the reaction is performed at 1100°C the pure 2222 phase is obtained (Fig. 6), although in some cases (mainly in the case of Ln = Nd) the formation of a very small amount of $BaTiO_3$ and/or Ln_2CuO_4 is difficult to avoid. Similar results were also reported for the syntheses of $Ln_2Ba_2Cu_2Ti_{2-x}Sn_xO_{11-\delta}$ (27, 35, 43), which led to impurities of $BaTiO_3/BaSnO_3$ or Ln_2CuO_4. We believe that all the quadruple perovskites belonging to this family have the same reaction pathway:

$$Ln_2O_3 + 2BaCO_3 + 2CuO + 2\,TiO_2$$
$$\downarrow -2CO_2$$

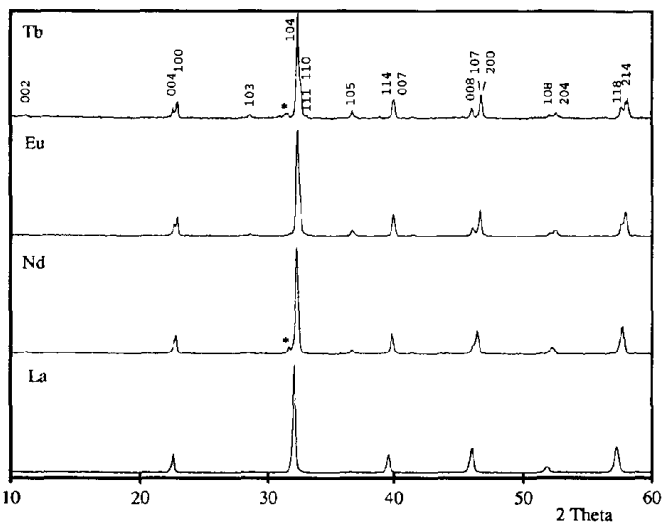

FIG. 6. X-ray diffraction patterns of $Ln_2Ba_2Cu_2Ti_2O_{11-\delta}$ (Ln = La, Nd, Eu, and Tb) synthesized at 1100°C. Impurities of Nd_2CuO_4 and $Tb_2Cu_2O_5$ are marked with an asterisk.

$$2\,BaTiO_3 + Ln_2CuO_4 + CuO$$
$$\downarrow$$
$$La_2Ba_2Cu_2Ti_2O_{11-\delta}.$$

The reaction has two steps: in the first ternary oxides are formed and in the second they react to form the final complex oxide. This path is indeed similar to the one we found for the formation of La_2CuTiO_6 (28–30). Thus, these studies seem to indicate that the high-temperature ceramic synthesis of complex oxides (containing three or four metals) does not lead to their direct formation, but proceeds through the formation of intermediate ternary oxides.

In the case of $Tb_2Ba_2Cu_2Ti_2O_{11-\delta}$ the 2222 phase obtained is almost pure except for a very small amount of $Ln_2Cu_2O_5$. On the other hand, attempts to synthesize $Ln_2Ba_2Cu_2Ti_2O_{11-\delta}$ with smaller lanthanides (*Ln* = Dy, Y) at 1100°C yielded only mixtures containing mainly $Ln_2Cu_2O_5$ and $BaTiO_3$.

The presence of small amounts of impurities that resist elimination could be explained by the proximity of a melting process with decomposition to the temperature of synthesis of these phases.

Concerning the nature of the possible impurities obtained, we have pointed out two different kinds of behavior in the reactions of synthesis of the 2222 phase: formation of the phase plus La_2CuO_4 + $BaTiO_3$ impurities (if any) in the case of La, Nd, or $Ln_2Cu_2O_5$ + $BaTiO_3$ impurities in the case of Tb. A possible reason for this varying behavior is the change in stability of Ln_2CuO_4 oxides, as reported by Tretyakov *et al.* (44): for lanthanides smaller than gadolinium the Ln_2CuO_4 structure is unstable with respect to the formation of $Ln_2Cu_2O_5$ (45, 46) under the synthesis conditions used. Thus, the reaction between Ln_2O_3 and CuO yields $Ln_2Cu_2O_5$ in the case of Tb, for which the overall reaction is:

$$Ln_2O_3 + 2\,BaCO_3 + 2\,CuO + 2\,TiO_2$$
$$\downarrow -2CO_2$$
$$2\,BaTiO_3 + Ln_2Cu_2O_5$$
$$\downarrow$$
$$La_2Ba_2Cu_2Ti_2O_{11-\delta}.$$

Finally, for lanthanides smaller than terbium the 2222-phase cannot be obtained. Even at 1100°C the products of the reaction are $Ln_2Cu_2O_5$ and $BaTiO_3$. We presume that, as the lanthanide becomes smaller, the 2222-type structure becomes less stable because the Ln^{3+} ion is too small to fit in this type of structure in combination with the large Ba^{2+} ion. In addition, the $Ln_2Cu_2O_5$ structure increases its thermodynamic stability with decreasing lanthanide radius and does not decompose until higher temperatures are reached (47), at which our reaction mixture has already melted. Therefore, it all results in the second step of the reaction path to form the 2222-type structure not taking place.

We have also studied the influence of the reaction time on obtaining the 2222 phase for *Ln* = La, Nd, and Eu. In the case of *Ln* = La the reaction seems to proceed faster, since after just 2 hr at 1100°C the 2222-phase is the major phase and La_2CuO_4 and $BaTiO_3$ are only present as impurities in very small amounts; after 6 hr the reaction is complete for the La derivative, whereas in the case of *Ln* = Nd and Eu, after 6 hr of reaction, small but still significant amounts of Ln_2CuO_4 and $BaTiO_3$ are still present in the reaction mixture.

Oxygen Content of $Ln_2Ba_2Cu_2Ti_2O_{11-\delta}$ Oxides

Thermogravimetric analyses on the $Ln_2Ba_2Cu_2Ti_2O_{11-\delta}$ oxides indicate an oxygen content between 10.94 and 10.97 ±0.02, depending on the sample and the lanthanide. For these thermogravimetric analyses samples were heated for 6 hr at 650°C under an Ar/H_2 atmosphere (5% H_2 v/v). The reaction taking place is

$$Ln_2Ba_2Cu_2Ti_2O_{11-\delta} + (2-\delta)H_2 \rightarrow$$
$$Ln_2O_3 + 2\,BaTiO_3 + 2\,Cu + (2-\delta)H_2O\uparrow$$

The solid decomposition products were identified by X-ray powder diffraction. So within experimental error, the oxygen content calculated from the thermogravimetric reduction is consistent with tetravalent titanium and divalent copper. TGA on oxygen-annealed samples (500°C) yields the same results. The very small oxygen deficiencies with respect to the nominal content of 11 detected by these analyses could in fact be associated with a small deficiency in copper due to partial fusion; this is consistent with the observation of small orange stains on the crucibles used for some preparations. We can therefore conclude that within experimental error the oxygen content of these samples corresponds to 11 oxygen atoms per formula unit.

Structure of $Ln_2Ba_2Cu_2Ti_2O_{11-\delta}$ Oxides

The oxides belonging to the general family $Ln_2Ba_2Cu_2Ti_2O_{11-\delta}$ present a perovskite-type structure with a "major superstructure" associated with the presence of a *c* axis four times that of a simple perovskite (a_p). We have previously reported this superstructure based on X-ray, electron diffraction, and HREM data (28, 32–34) and have also published a neutron diffraction study on the La

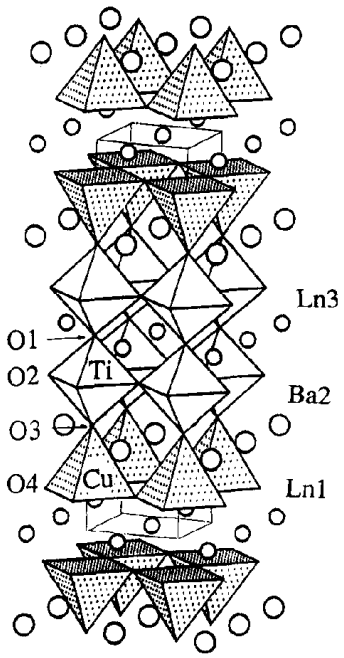

FIG. 7. Crystal structure of $Ln_2Ba_2Cu_2Ti_2O_{11-\delta}$. Copper occupies the pyramidal position whereas titanium has an octahedral coordination to oxygen. Note the additional ordering of *Ln* and Ba ions.

and Nd derivatives (48). Figure 7 shows this structure, which is related to the perovskite ($A_nB_nO_{3n}$) but contains one oxygen vacancy per formula unit. This leads to two different coordination sites for the transition metals, namely square pyramidal (occupied by copper) and octahedral (occupied by titanium), and in turn leads also to three possible sites for the lanthanides and barium ions, which are also ordered within the structure (33).

This structural model has been confirmed by neutron diffraction on the lanthanum and neodymium derivatives. Both of them present the tetragonal superstructure, though the lanthanum derivative presents only partial order of the cations consistent with the existence of ordered microdomains. For the neodymium derivative though, and by extension for the smaller lanthanide derivatives, the order of oxygen vacancies and cations (both Cu/Ti and *Ln*/Ba pairs) is found to extend to long range (48).

The already mentioned $a_p \times a_p \times 4a_p$ superstructure can be clearly observed both in electron diffraction patterns (Fig. 8) and in low resolution images (Fig. 9). Comparison of the latter for the La and Nd derivatives shows that the layered structure of the former is much more affected by defects; this less perfect order was anticipated from the weakness of the superstructure spots for the lanthanum derivative, and was also confirmed by neutron profile analyses (48). But electron diffraction studies also reveal other interesting structural features. In the case of $La_2Ba_2Cu_2Ti_2O_{11-\delta}$ the structure corresponds effectively to just an $a_p \times a_p \times 4a_p$ cell and the extinction symbol consistent with the systematic absences observed is *P*---. In this sense, $La_2Ba_2Cu_2Ti_2O_{11-\delta}$ differs from $La_2Ba_2Cu_2Sn_2O_{11-\delta}$, for which an additional superstructure is observed. On the other hand, the oxides $Ln_2Ba_2Cu_2Ti_2O_{11-\delta}$ (*Ln* = Nd, Eu, Tb) do indeed present an additional "minor superstructure" that forces a redefinition of the unit cell to $\sqrt{2}a_p \times \sqrt{2}a_p \times 8a_p$ in order to be able to index all the spots in the patterns (see Fig. 10). This superstructure is similar to that described for $La_2Ba_2Cu_2Sn_2O_{11-\delta}$ (27), which presented nevertheless a longer *c* axis ($\sqrt{2}a_p \times \sqrt{2}a_p \times 24a_p$). Within the series $Ln_2Ba_2Cu_2Ti_2O_{11-\delta}$ (*Ln* = Nd, Eu, Tb), the minor superstructure is more clearly observed in $[310]_p$ patterns for *Ln* = Eu and *Ln* = Tb whereas for *Ln* = Nd diffusion streaks are observed instead of well defined spots (Fig. 10b). The definition of the spots changes from crystal to crystal, though the general trend is toward better defined spots as the lanthanide ionic radius decreases.

In the case of *Ln* = Eu and more commonly for *Ln* = Tb weak spots at 1/2(110) in the $[001]_p$ and $[011]_p$ patterns are also observed for thick crystals (Figs. 8f and 10d). This forces us to consider the existence of two different types of crystals for $Ln_2Ba_2Cu_2Ti_2O_{11-\delta}$ (*Ln* = Eu, Tb) with different space groups: Type 1 crystals include all crystals of the Nd derivative and most of the Eu derivative studied belong to this type; these crystals show no additional spots on the [001] pattern (Fig. 8e) (extinction symbol *I*-c-). Type 2 crystals, where weak spots appear on the [001] (Fig. 8f) and $[012]_p$ patterns (extinction symbol *P*--*c*), are predominant for *Ln* = Tb.

In the case of $La_2Ba_2Cu_2Sn_2O_{11-\delta}$ the presence of analog superstructure spots, indicating a $\sqrt{2}a_p \times \sqrt{2}a_p \times 24a_p$ supercell, was also found and assigned to the rotation of the SnO_6 polyhedra around [001] to compensate for the copper–tin size mismatch. Among superconducting oxides with perovskite structure, typical copper–copper separations within a CuO_2 layer ranges from 3.80 to 3.85 Å (49) whereas typical tin-tin separations are 4.1 Å (27). On the other hand, in the case of titanium, values between 3.90 and 3.95 Å are commonly found (50–52) so the layer mismatch is much smaller than in the case of the tin compound.

The existence of the additional minor superstructure could also be related to a difference in size between different components of the structure. As we have already pointed out, a minor superstructure exists for the lanthanum derivative of the copper–tin perovskite, but in the case of the analog copper–titanium oxides a similar superstructure appears only for derivatives with smaller lanthanides. This can be associated to a size mismatch between tin or titanium and the neighboring lanthanide ions. To illustrate this explanation, we have calculated a ratio *r*, mathematically identical to a tolerance factor, but which

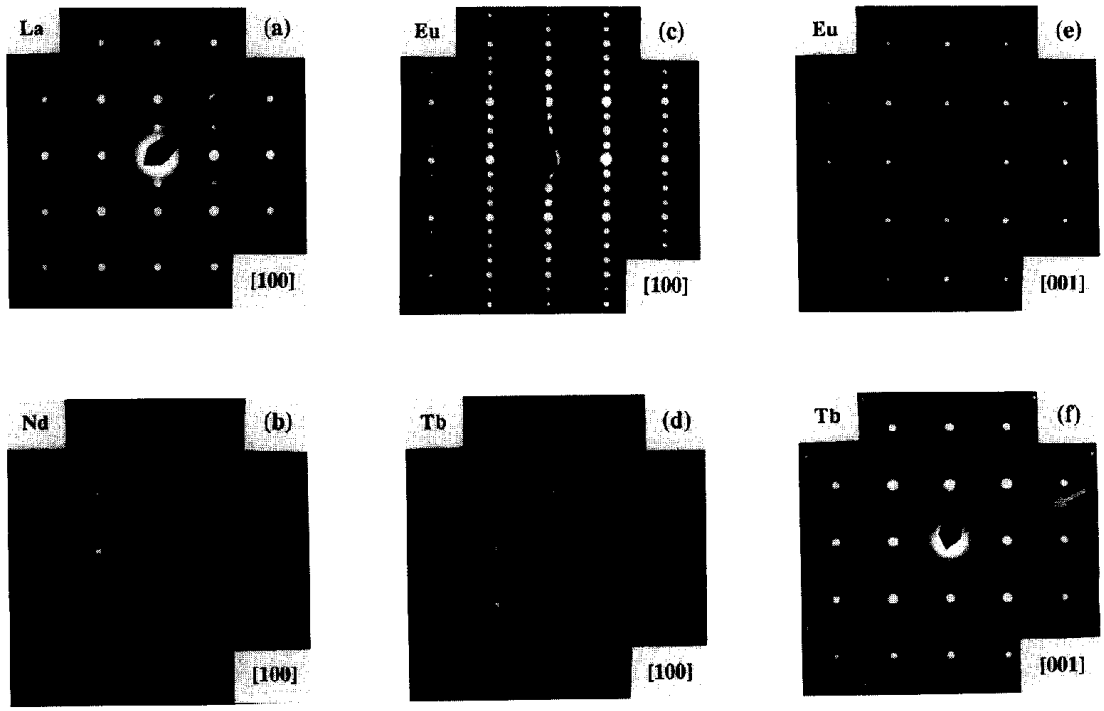

FIG. 8. Electron diffraction pattern corresponding to $Ln_2Ba_2Cu_2Ti_2O_{11-\delta}$ for the indicated zone axis. Additional spots in the [001] pattern in the case of the terbium derivative are marked with an arrow.

is intended in this case just to show the degree of size mismatch: $r = (R_A + R_O)/(\sqrt{2} \times (R_B + R_O)$, where R_A, R_B, and R_O are the ionic radii for A, B, and oxygen with respective coordination numbers 12, 6, and 2 (53). The values obtained are: A = La, B = Sn, $r = 0.939$; A = La, B = Ti, $r = 0.980$; and A = Nd, B = Ti, $R = 0.948$. We can see how the compound with the highest r value, approaching 1 ($La_2Ba_2Cu_2Ti_2O_{11-\delta}$), is the only one not presenting the minor superstructure. Therefore it seems reasonable to suppose that the distortion leading to the existence of the minor superstructure appears only for small values of r, or in other words when the size mis-

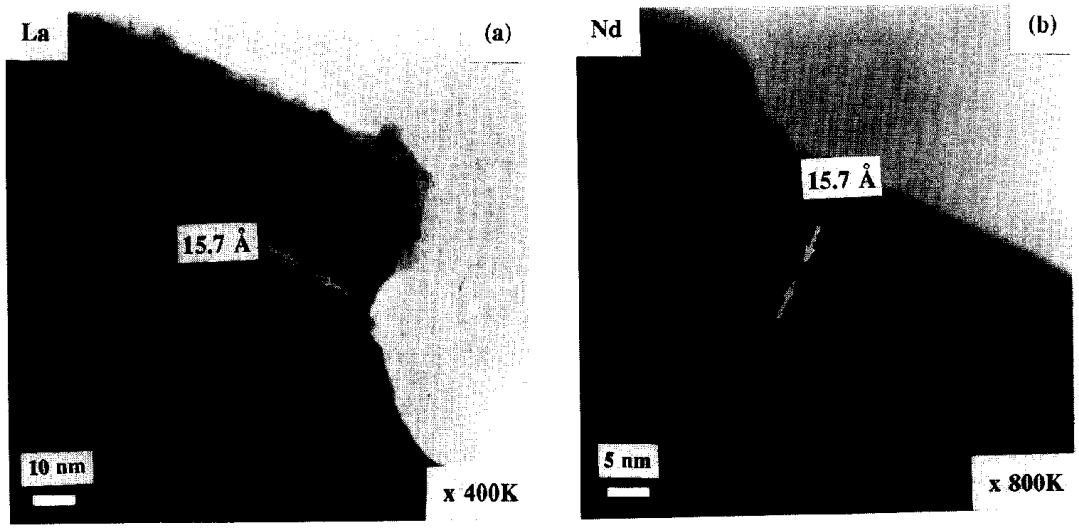

FIG. 9. Low-resolution images for $Ln_2Ba_2Cu_2Ti_2O_{11-\delta}$, with (a) Ln = La and (b) Ln = Nd, corresponding to the [100] zone axis. Although the lanthanum derivative presents a less ordered arrangement, its layered structure is evidenced.

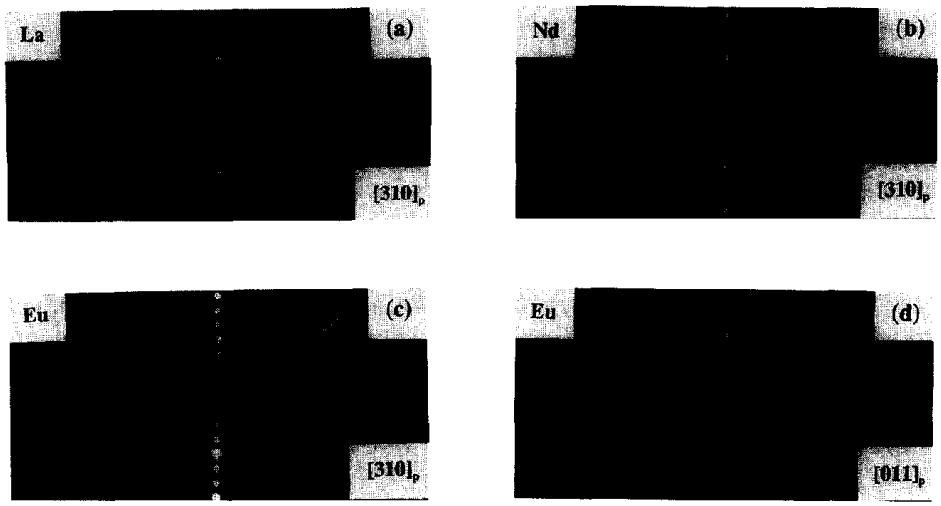

FIG. 10. Electron diffraction pattern corresponding to $Ln_2Ba_2Cu_2Ti_2O_{11-\delta}$ for the zone axis indicated. Additional spots which force a definition of a $\sqrt{2}a_p \times \sqrt{2}a_p \times 8a_p$ unit cell for all lanthanides except lanthanum are indicated with an arrow.

match between A and the BO_6 perovskite framework is large. For sufficiently small r values one could expect the corresponding compound to be unstable; this has been found to be the case for a hypothetical yttrium 2222 derivative where the mixture of binary oxides seems to be thermodynamically more stable.

Discussion on the Structure and Stability of Quadruple Perovskites

Through the work of Poeppelmeïer and co-workers on Cu–Sn perovskites and more recently with the independent reports on Cu–Ti perovskites made by Weller and co-workers and by ourselves, a new class of layered mixed perovskites with the superstructure described above is emerging. Thus, this major $a_p \times a_p \times 4a_p$ superstructure has been detected on compounds with the general formula $Ln_2Ba_2Cu_2B_2O_{11-\delta}$ by Gormezano and Weller (by means of Rietveld X-ray refinements) in the case of Ln = Gd and B = Ti (35), Ln = Nd and B = Sn : Ti (1 : 1), and Ln = Sm and B = Sn : Ti (1 : 3) (43), by Anderson *et al.* in the case Ln = La and B = Sn (27) and by ourselves in the case of Ln = Nd, Eu, Tb and B = Ti (28, 32–34, 48). In the case of $La_2Ba_2Cu_2Ti_2O_{11-\delta}$ the $4a_p$ superstructure can only be detected by means of neutron or electron diffraction, with the X-ray pattern being identical to that of a simple perovskite. This is probably why Gormezano and Weller reported that a layered lanthanum derivative could not be obtained (35). The maxima corresponding to superstructure reflections are weaker than for other derivatives but can be clearly and unambiguously detected on the corresponding electron diffraction patterns and on the neutron diffraction pattern of the lanthanum derivative prepared by us.

Concerning the stability of these quadruple perovskites, it has been proposed that there is a very narrow range of stability between values of an "average" tolerance factor (43) $t_{av.} = [r_O + (r_{A'} + r_{A''})/2]/\sqrt{2}[r_O + (r_{B'} + r_{B''})/2]$ such that the quadruple perovskite would be stable only for $0.97 \geq t_{av.} \geq 0.965$ (54). Our results clearly contradict this proposal and show that a relatively large variety of lanthanides with different ionic radii (56) are compatible with the formation of the quadruple perovskite superstructure in the system Ln–Ba–Cu–Ti. Therefore, the introduction of Sn on the structure to compensate for larger Ln ions (such as Nd) as reported in Ref. (43), though possibly leading to less stressed structures, is clearly not necessary for the formation of the layered superstructure.

Structural Correlations in Quadruple Perovskites

From X-ray and neutron diffraction studies, many structural parameters of interest can be extracted by means of Rietveld profile analyses. In addition to unit cell dimensions and/or distortions, we have analyzed chemically significant parameters such as the coordination polyhedra of copper ions in the structure and report here the structural correlations found among the several oxides studied.

The cell parameters obtained from X-ray powder diffraction patterns are shown in Table 1. This table summarizes literature data from the gadolinium derivative (35) and our own on lanthanum, neodymium, europium, and terbium derivatives. We must note that the X-ray data for the lanthanum derivative could also be fitted with cubic symmetry and a = 3.9464(1) Å.

As could be expected, parameter a is found to decrease with the lanthanide ionic radius (56) (see Fig. 11a). We

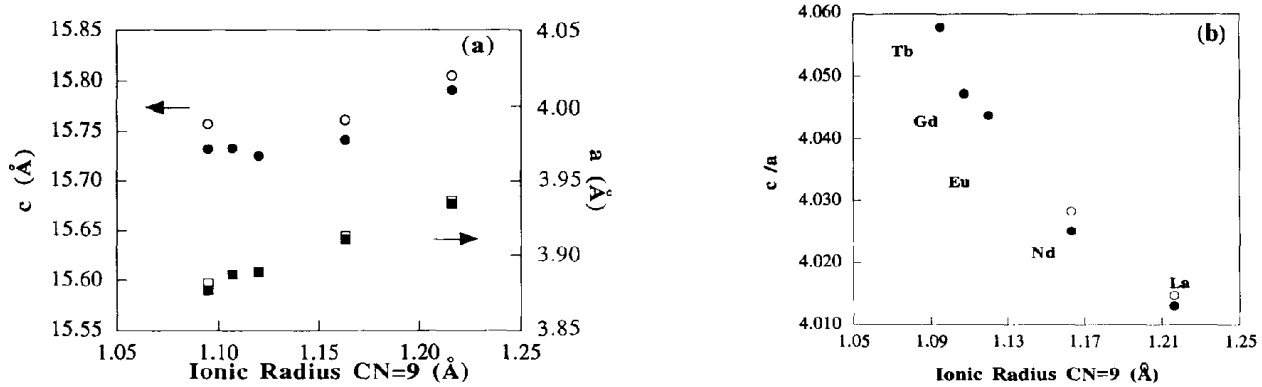

FIG. 11. Plot of (a) parameters c and a and (b) degree of tetragonal distortion expressed as c/a for $Ln_2Ba_2Cu_2Ti_2O_{11-\delta}$ versus the ionic radius of the lanthanide for a coordination number of 9 (note that the true coordinations are 8 and 12, but the absence of several relevant data in (53) made us select these values to allow a meaningful, though relative, comparison. With decreasing lanthanide radius, parameters a and c decrease and the tetragonal distortion increases. Data for Ln = Gd are taken from ref. (35). Empty symbols correspond to neutron diffraction and filled symbols to X-ray diffraction data.

have previously mentioned the existence of a small mismatch between the copper and titanium layers. That mismatch would force the former to expand and the latter to contract in order to accommodate themselves in the structure. In this sense, a decrease in the radius of the lanthanide allows for a decrease in the titanium–titanium separation (and hence in the a parameter), thus diminishing the mismatch. On the other hand, the c parameter does not follow a linear trend, but already seems to reach a "minimum of compressibility" for the europium derivative (Fig. 11a). This behavior is similar to what is found for the $LnBa_2Cu_3O_{7-\delta}$ series for Ln = La, Pr, Nd, Sm, Eu, Gd, Dy, Ho, Er, Tm, Yb, and Lu (57). Finally, the degree of tetragonal distortion, as indicated by the c/a ratio, increases as the lanthanide radius decreases (Fig. 11b), thus following the trend observed in the previous calculation of the r factors.

Among the structural correlations derived from X-ray Rietveld analyses of several oxides, we must remark upon the relation between the lanthanide ionic radii and $Cu–O_{equatorial}$ bond lengths, given the central effect of these on superconducting properties of layered cuprates. Thus, Fig. 12 shows a clear overall correspondence between this bond length and the lanthanide size. A comparison of the above data for Ln = La with the $Cu–O_{eq.}$ bond length of 2.007(1) Å reported for the Cu–Sn perovskite shows the significant decrease in this important parameter attained in going from the tin to the titanium cuprates. Furthermore, within the series of titanium cuprates, the shortest $Cu–O_{eq.}$ bond of 1.947(3) Å (combined with a larger $Cu–O_{eq.}$–Cu angle of 169(1)°) found in the case of the terbium derivative makes that system the best candidate for high-T_c superconductivity provided adequate p doping is achieved. In principle, an extension to smaller lanthanide (down to yttrium) would be desirable, but according to our results is not possible.

TABLE 1
Cell Parameters (from X-Ray Data) for the Series $Ln_2Ba_2Cu_2Ti_2O_{11}$

Ln	a (Å)	c (Å)	c/a
La	3.9348(2)	15.791(2)	4.013
Nd	3.9106(2)	15.741(2)	4.025
Eu	3.8889(3)	15.726(2)	4.044
Gd[a]	3.8873(2)	15.7335(7)	4.047
Tb	3.8795(5)	15.744(3)	4.058

Note. The degree of tetragonality is given by the ratio c/a.
[a] From Ref. (35).

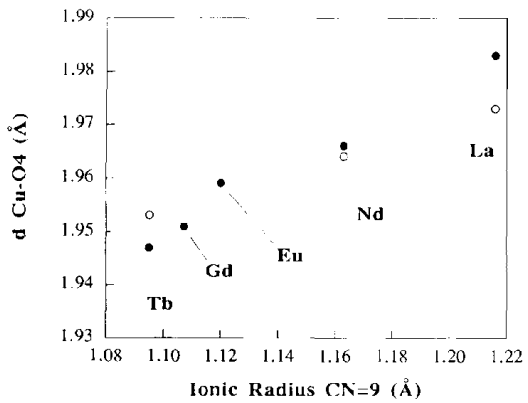

FIG. 12. Plot of $Cu–O_{eq}$ bond distance versus the ionic radius of the lanthanide for $Ln_2Ba_2Cu_2Ti_2O_{11-\delta}$. Empty symbols correspond to neutron diffraction and filled symbols to X-ray diffraction data.

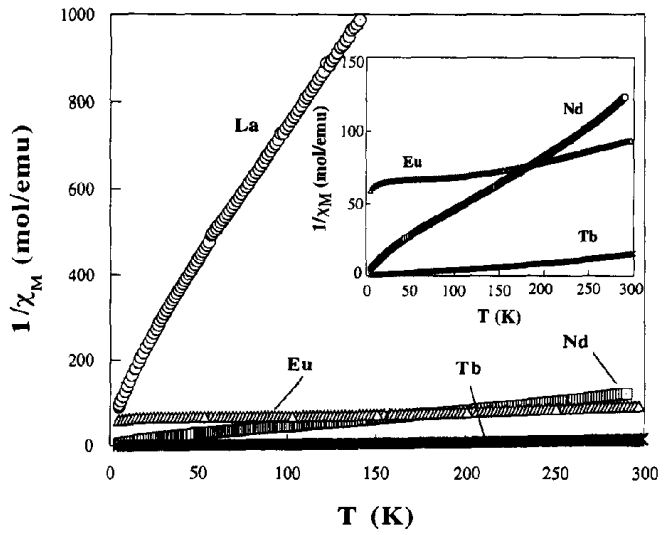

FIG. 13. Plot of the inverse of the susceptibility versus T for $Ln_2Ba_2Cu_2Ti_2O_{11-\delta}$. The inset shows an expanded plot where irregular behavior at low temperatures can be seen in the case of Ln = Nd, Eu, and Tb.

Magnetic Properties

Susceptibility data for $Ln_2Ba_2Cu_2Ti_2O_{11-\delta}$ (Ln = La, Nd, Eu, and Tb) at high temperatures can be fitted with good agreement to a Curie–Weiss law. Figure 13 shows the graphics of $1/\chi$ vs T, where linear behavior at high temperatures is observed. However, at low temperatures curvatures do appear in the case of Ln = Nd and Eu, which are more clearly seen in expanded graphs (see inset of Fig. 13). This complex behavior is due to the magnetic moments of neodymium and europium that present a complex dependence on temperature (58). On the other hand, in the case of the lanthanum derivative the behavior of $1/\chi$ vs T is simpler and closer to a Curie–Weiss law due to the fact that all magnetic contributions come from Cu(II) ions and hence the values of the effective magnetic moment are the lowest of the whole family. The values of the effective magnetic moment per copper atom at room temperature for $Ln_2Ba_2Cu_2Ti_2O_{11-\delta}$ are: μ_{eff} per Cu (μ_B) 0.81 (Ln = La), 3.07 (Nd), 3.52 (Eu), and 8.59 (Tb).

The magnetic susceptibility data for $La_2Ba_2Cu_2Ti_2O_{11-\delta}$ and La_2CuTiO_6 are directly comparable once normalized with respect to the number of copper atoms per formula unit. Figure 14 shows the plot of $1/\chi$ vs T for both oxides. $La_2Ba_2Cu_2Ti_2O_{11-\delta}$ shows a smaller curvature localized at lower temperatures whereas for La_2CuTiO_6 the curvature is extended to the whole temperature range and does not correspond to a simple Curie–Weiss law (28). For $La_2Ba_2Cu_2Ti_2O_{11-\delta}$, data above 50 K can be fitted to a Curie–Weiss law ($\chi = C/\theta + T$) with C = 0.1752 emu · K/mole (C = 0.088 emu K/mole per copper atom) and θ = 31 K with R = 0.9971 (see Fig. 14). These parameters do not change significantly when the fit is constrained to data above 100 K. The fact that μ_{eff} per copper atom (μ_B) for $La_2Ba_2Cu_2Ti_2O_{11-\delta}$ is lower than for La_2CuTiO_6 in the whole temperature range indicates that the former exhibits a stronger antiferromagnetic coupling. The comparison of the values of the effective magnetic moment obtained for this compound and for other perovskite-type oxides with different degrees of order between copper and titanium also indicates the presence of this strong coupling which is consistent with the presence of CuO_2 planes and hence with the ordering of copper and titanium. As an example the magnetic moment of the layered oxide $Y_{0.8}Ca_{0.2}Sr_2Cu_2GaO_7$ which contains CuO_2 planes is 0.8 μ_B (11), very close to the value of 0.81 obtained for our La derivative, and clearly smaller than the spin-only value corresponding to ideally isolated Cu(II) ions ($\mu_{spin\ only}$ = 1.75 μ_B) or to the value of 1.14 μ_B found for the disordered perovskite La_2CuTiO_6 (28, 29).

Doping of the Series $Ln_2Ba_2Cu_2Ti_2O_{11}$

The final stage of our study of these layered titanium cuprates is the preparation of doped derivatives in order to induce conductivity or superconductivity. In spite of the several doping strategies possible this process is proving not trivial in these oxides. The first and most elemental approach for preparing solid solutions of the type $Ln_{2-x}Ba_{2+x}Cu_2Ti_2O_{11}$ or doped derivatives such as $Ln_{2-x}A_xBa_2Cu_2Ti_2O_{11}$ (A = Sr, Ca) were not successful. Similarly to the analogous Cu–Sn quadruple perovskite, these phases seem to occupy just a point (or a very narrow area) on the corresponding phase diagram. On the other hand, we have tried with some success to substitute aliovalent ions for titanium in these oxides and are presently working in this direction.

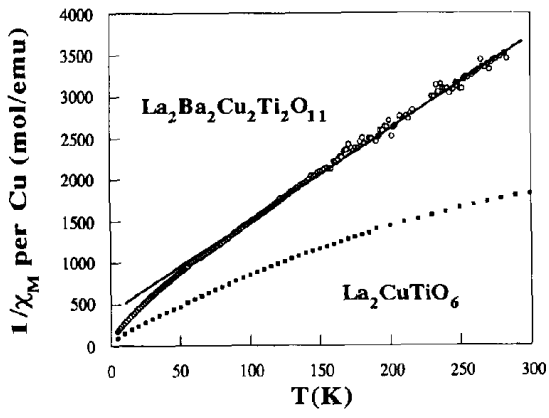

FIG. 14. Plot of the inverse of the susceptibility versus T for $La_2Ba_2Cu_2Ti_2O_{11-\delta}$ and La_2CuTiO_6. The data above 50 K for the former can be fitted to a Curie–Weiss law.

CONCLUSIONS

Extensive research on the synthesis of layered titanium cuprates in the system *Ln*–(Ba/Sr)–Cu–Ti–O has led to the discovery of several new interesting phases. On the one hand, samples with nominal compositions $Ln(Ba/Sr)_2Cu_2TiO_{8-\delta}$ do not yield pure products, presumably due to the high formal oxidation state required for copper in the hypothetical perovskite structure. As part of this research though, and confirming previous reports, a bulk superconducting oxide (T_c onset of 26 K, 80% Meissner fraction) with composition $YSr_2Cu_{2.7}Ti_{0.3}O_{8-\delta}$ and an $a_p \times a_p \times 3a_p$ superstructure was isolated and characterized.

On the other hand a whole new family of oxides of formula $Ln_2Ba_2Cu_2Ti_2O_{11-\delta}$ has been characterized and its range of existence for lanthanides between La and Tb determined. For smaller lanthanides, mixtures containing $Ln_2Cu_2O_5$ and $BaTiO_5$ were obtained. Thus, this remarkable structure proves to be stable for a relatively wide range of *Ln* ionic radii. These oxides present a tetragonal distortion that increases as the size of the lanthanide decreases; a major $a_p \times a_p \times 4a_p$ superstructure is also present in all cases, though for the La derivative the superstructure peaks are weaker. An additional minor superstructure ($\sqrt{2}a_p \times \sqrt{2}a_p \times 8a_p$) is observed for the smaller lanthanide derivatives.

Concerning structural parameters relevant to superconductivity, the $Cu–O_{eq.}$ bond distance decreases along the series and a minimum value of 1.947(3) Å is found for the terbium derivative. This value represents a substantial shortening with respect to that found for the related copper–tin quadruple perovskite $La_2Ba_2Cu_2Sn_2O_{11}$ (2.007(1) Å) and therefore represents a further step in the optimization of the quadruple perovskites structure toward superconductivity.

ACKNOWLEDGMENTS

Financial support by the Spanish DIGICYT (PB93-0122), CICYT (MAT93-0240-C04-01) and the MIDAS Program (93-2331) is gratefully acknowledged. We thank Dr. J. L. García and A. Gou for the measurements performed on the superconducting samples, and the Generalitat de Catalunya for a predoctoral fellowship to M.R.P.

REFERENCES

1. M. K. Wu, J. R. Ashburn, C. J. Torng, P. H. Hor, R. L. Meng, L. Gao, Z. J. Huang, Y. Q. Wang, and C. W. Chu, *Phys. Rev. Lett.* **58,** 908 (1987).
2. N. Murayama, E. Sudo, K. Kani, A. Tsuzuki, S. Kawakami, M. Awano, and Y. Torii, *Jpn. J. Appl. Phys.* **27**(9), L1623 (1988).
3. C. Greaves and P. R. Slater, *Physica C* **161,** 245 (1989).
4. M. J. Rey, P. Dehaudt, J. Joubert, and A. W. Hewat, *Physica C* **167,** 162 (1990).
5. C. Greaves and P. R. Slater, *IEEE Trans. Magn.* **27**(2), 1174 (1991).
6. H. W. Zandbergen, R. J. Cava, J. J. Krajewski, and W. F. Peck Jr., *J. Solid State Chem.* **101,** 322 (1992).
7. B. Hellebrand, X. Z. Wang, and P. L. Steger, *J. Solid State Chem.* **110,** 32 (1994).
8. S. A. Sunshine, L. F. Schneemeyer, T. Siegrist, D. C. Douglass, J. V. Waszczak, R. J. Cava, E. M. Gyorgy, and D. W. Murphy, *Chem. Mater.* **1,** 331 (1989).
9. (a) P. R. Slater and C. Greaves, *Physica C* **180,** 299 (1991); (b) E. Suard, V. Caignaert, A. Maignan, and B. Raveau, *Physica C* **182,** 219 (1991); (c) V. Caignaert *et al. J. Solid State Chem.* **109,** 295 (1994).
10. G. Roth, P. Adelmann, G. Heger, R. Knitter, and Th. Wolf, *J. Phys. I France* **1,** 721 (1991).
11. J. T. Vaughey, J. P. Thiel, E. F. Hasty, D. A. Groenke, C. L. Stern, K. R. Poeppelmeier, B. Dabrowski, D. G. Hinks, and A. W. Mitchell, *Chem. Mater.* **3,** 935 (1991).
12. T. A. Mary, N. R. S Kumar, and U. V. Varadaraju, *J. Solid State Chem.* **107,** 524 (1993).
13. T. Krekels, O. Milat, G. Van Tendeloo, S. Amelinckx, T. G. N. Babu, A. J. Wright, and C. Greaves, *J. Solid State Chem.* **105,** 313 (1993).
14. P. F. Miceli, J. M. Tarascon, L. H. Greene, P. Barboux, F. J. Rotella, and J. D. Jorgensen, *Phys. Rev. B* **37,** 5932 (1988).
15. Y. K. Tao, J. S. Swinnea, A. Manthiram, J. S. Kim, J. B. Goodenough, and H. Steinfink, *J. Mater. Res.* **3,** 248 (1988).
16. M. S. Hedge, K. M. Satyalakshmi, S. Ramesh, N. Y. Vasanthacharya, and J. Gopalakrishnan, *Mater. Res. Bull.* **27,** 1099 (1992).
17. Q. Huang, R. J. Cava, A. Santoro, J. J. Krajewski, and W. F. Peck, *Physica C* **193,** 196 (1992).
18. E. García-González, M. Parras, J. M. González-Calbet, and M. Vallet-Regí, *J. Solid State Chem.* **104,** 232 (1993).
19. E. García-González, M. Parras, J. M. González-Calbet, and M. Vallet-Regí, *J. Solid State Chem.* **105,** 363 (1993).
20. E. García-González, M. Parras, J. M. González-Calbet, and M. Vallet-Regí, *J. Solid State Chem.* **110,** 142 (1994).
21. (a) L. Er-Rakho, C. Michel, Ph. Lacorre, and B. Raveau, *J. Solid State Chem.* **73,** 531 (1988); (b) V. Caignaert, I. Mirebeau, F. Bouree, N. Nguyen, A. Ducouret, J-M. Greneche, and B. Raveau, *J. Solid State Chem.* **114,** 24 (1995).
22. M. Pissas, C. Mitros, G. Kallias, V. Psycharris, A. Simopoulos, A. Koufoudakis, and D. Niarchos, *Physica C* **192,** 35 (1992).
23. M. J. Ruiz-Aragón, C. Rial, E. Morán, J. B. Torrance, N. Menéndez, and J. B. Tornero, *Solid State Ionics* **63–65,** 932 (1993).
24. C. T. Lin, S. X. Li, W. Zhou, A. Mackenzie, and W. Y. Liang, *Physica C* **176,** 285 (1991).
25. W. Zhou, *Chem. Mater.* **6,** 441 (1994).
26. M. T. Anderson and K. R. Poeppelmeier. *Chem. Mater.* **3,** 476 (1991).
27. M. T. Anderson, K. R. Poeppelmeier, J.-P. Zhang, H.-J. Fan, and L. D. Marks, *Chem. Mater.* **4,** 1305 (1992).
28. M. R. Palacín, Masters Thesis, Universitat Autònoma de Barcelona, October 1993.
29. P. Gómez-Romero, M. R. Palacín, N. Casañ, A. Fuertes, and B. Martínez, *Solid State Ionics* **63–65,** 424 (1993).
30. M. R. Palacín, J. Bassas, J. Rodríguez-Carvajal, and P. Gómez-Romero, *J. Mater. Chem.* **3**(11), 1171 (1993).
31. M. R. Palacín, A. Fuertes, N. Casañ-Pastor, and P. Gómez-Romero, *Mater. Res. Bull.* **29**(9), 973 (1994).
32. M. R. Palacín, A. Fuertes, N. Casañ-Pastor, and P. Gómez-Romero, Presented at IV Reunión Nacional de Materiales Oviedo, Spain October 19–21 1993.
33. M. R. Palacín, A. Fuertes, N. Casañ-Pastor, and P. Gómez-Romero, *Adv. Mater.* **6**(1), 54 (1994).
34. M. R. Palacín, F. Krumeich, M. T. Caldés, and P. Gómez-Romero. *J. Solid State Chem.* **117,** 213 (1995).
35. A. Gormezano and M.T. Weller. *J. Mater. Chem.* **3**(7), 771 (1993).
36. C. E. Hamrin Jr., W. D. Arnett, R. J. De Angelis, X. X. Ding, and W. D. Ehmann, *Solid State Commun* **69**(11), 1063 (1989).

37. (a) T. Den and T. Kobayashi, *Physica C* **196** 141 (1992); (b) S. J. Wuu, D. H. Chen, T. W. Liu, C. H. Cheng, C. T. Chang, S. R. Sheen, and M. K. Wu, *Physica C* **226,** 37 (1994).
38. T. A. Mary and U. V. Varadaraju, *Physica C* **215,** 269 (1993).
39. T. Wada, N. Suzuki, A. Maeda, T. Yabei, K. Uchinokura, S. Uchida, and S. Tanaka, *Phys. Rev. B* **39**(13), 9126 (1989).
40. D. V. Formichev, O. G. D'yachenko, A. V. Mironov, and E. V. Antipov, *Physica C* **225,** 25 (1994).
41. P. R. Slater and C. Greaves, *Physica C* **180,** 299 (1991).
42. V. P. N. Padmanaban and K. Shahi, *Physica C* **208,** 263 (1993).
43. A. Gormezano and M. T. Weller, *J. Mater. Chem.* **3**(9), 979 (1993).
44. Y. D. Tretyakov, A. R. Kaul, and N. V. Makukhin, *J. Solid State Chem.* **17,** 183 (1976).
45. W. Wong-Ng, *Powder Diffr.* **7**(3), 125 (1992).
46. E. Takayama-Muromachi and A. Navrotsky, *J. Solid State Chem.* **106,** 349 (1993).
47. T. Mathews and K. T. Jacob, *J. Mater. Res.* **8**(12), 3015 (1993).
48. P. Gómez-Romero, M. R. Palacín, and J. Rodríguez-Carvajal, *Chem. Mater.* **6**(11), 2118 (1994).
49. C. P. Poole Jr., T. Datta, and H. A. Farach, "Copper Oxide Superconductors," Chap. VI. Wiley–Interscience, New York, 1988.
50. J. E. Sunstrom IV, S. M. Kauzlarich, and P. Klavins, *Chem. Mater.* **4**(2), 346 (1992).
51. C. Eylem, G. Sàghi-Szabó, B. H. Chen, B. Eichhorn, J. L. Peng, R. Greene, L. Salamanca-Riba, and S. Nahm, *Chem. Mater.* **4**(5), 1038 (1992).
52. J. E. Sunstrom IV and S. M. Kauzlarich, *Chem. Mater.* **5**(10), 1539 (1993).
53. R. D. Shannon, *Acta Crystallogr. Sect. A* **32,** 751 (1976).
54. It must be noted that an averaging of ionic radii such as that proposed could be useful in predicting certain structures where ions A',A'' and B',B'' would be homogeneously distributed (see for example (55)). On the other hand, for a well ordered layered structure like the one at hand the averaging of ionic radii of atoms segregated onto layers is probably not adequate (i.e., this structure would not be formed for a combination of very large A' and B' ions and very small A'' and B'' ions, no matter how close to unity their $t_{av.}$ would come, due precisely to the layer mismatch problem).
55. F.S. Galasso, "Perovskites and High Tc Superconductors" Gordon & Breach, New York, 1990.
56. We have obtained the ionic radii values from Ref. (53). We must note though that in our figures and correlations, we have used the ionic radii of the lanthanide ions for a coordination number of 9. The true coordination numbers are 8 and 12 for sites 1 and 3, respectively, but the absence of several relevant data in this reference made us select the 9 values to allow a meaningful comparison. Thus, those values are not to be taken as absolute points of reference. Furthermore, a meaningful comparison with the data reported in Ref. (43) as a function of ionic radii was not possible due to the apparent discrepancies of the latter with those found in the 1976 work by Shannon (Ref. (53)).
57. A. V. Narlikar, C. V. Narashima Rao, and S. K. Agarwal, in "Studies of High Temperature Superconductors," Vol. 1, Chap. 15. (A. Narlikar, Ed.), Nova Science, New York, 1989.
58. T. H. Siddal, III *in* "Theory and Applications of Molecular Paramagnetism" (E. A Boudreaux and L. N. Mulay, Eds.), Chap. 5, Wiley, New York, 1976.